Proceedings of the Seventh International Conference on
Railway Technology: Research, Development and Maintenance
Edited by: J. Pombo
Civil-Comp Conferences, Volume 15, Paper 18.12
Civil-Comp Press, Edinburgh, United Kingdom, 2026
ISSN: 2753-3239, doi: 10.4203/ccc.15.18.12

Comparative Analysis of Railway Lateral Acceleration Using Inertial Measurement Unit and Global Navigation Satellite System

M. Espindola[1,2] and P. Kurka[2]

[1] Federal Institute of Sao Paulo - IFSP, Brazil
[2] School of Mechanical Engineering - FEM/UNICAMP, Brazil

Abstract

This paper presents a comparative analysis of lateral acceleration estimation in railway environments using three information sources: measurements from a triaxial accelerometer and heading information from the gyroscope of an Inertial Measurement Unit (IMU), and kinematic estimations derived from data from a Global Navigation Satellite System (GNSS). The proposed methodology incorporates a decimation and filtering procedure to synchronize high-frequency IMU data streams with lower-frequency GNSS measurements, thus establishing a common spatial and temporal reference framework. This study validates the framework using an open-access experimental railway dataset. The results confirm the physical consistency of all three estimation strategies and characterize their respective sensitivities to track curvature, geometric irregularities, and sensor noise. In general, the study provides a transparent, physics-based alternative to black-box machine-learning approaches for railway diagnostics.

Keywords: lateral acceleration, inertial measurement unit, global navigation satellite system, gyroscope heading, decimation filtering, railway monitoring, digital signal processing.

1 Introduction

Effective management of railway infrastructure requires continuous monitoring of the geometry of the track and the health of the rolling-stock to maintain operational safety, passenger comfort, and cost efficiency [1, 2]. Modern instrumented measurement vehicles address these demands by integrating global navigation satellite systems (GNSS) for spatial localization with inertial measurement units (IMU) that capture multi-axis accelerations and angular rates [3, 4].

Lateral acceleration constitutes a primary indicator of the dynamic behavior of the railway vehicle and the quality of the track geometry. Elevated or anomalous values of lateral acceleration directly indicate irregularity in track curvature, rail head wear, superelevation defects, and vehicle dynamic instability [2, 5]. Despite its relevance, robust estimation of acceleration from onboard sensor suites remains technically challenging. IMU capture high-frequency dynamic responses, frequently exceeding 100 Hz. Readings from GNSS receivers can be converted into accelerations that might indicate kinematic interactions between the railway and traveling vehicles. Commercially available GNSS receivers commonly operate at relatively low sampling frequencies (1–10 Hz) . This pronounced discrepancy in sampling rates, in conjunction with the use of different coordinate reference frames and the distinct underlying physical measurement principles, substantially complicates the direct comparison of accelerations between IMU sensors and GNSS estimates [6, 7].

In this context, the present work proposes a signal-processing methodology that conditions and compares all three lateral acceleration estimation paths, with particular emphasis on the decimation filtering procedure required to harmonize the disparate sensor sampling rates. This procedure that uses physics-based deterministic signal processing pipelines contrasts with Machine Learning (ML) and Artificial Intelligence (AI) strategies that rely on high-fidelity training datasets and are susceptible to physically inconsistent outputs [8, 9].

The specific objectives of this paper are to develop a signal-processing framework that transforms discrete GNSS position measurements into continuous lateral acceleration signals that are directly comparable to raw inertial measurements obtained from accelerometers and gyroscopes. A decimation and filtering procedure is used to temporally and spatially align and synchronize the IMU and GNSS data, allowing for a rigorous comparison of acceleration estimates derived from these two distinct classes of sensors. Data from gyroscope readings are also combined with GNSS estimated traveling velocities, to yield alternative estimates of lateral accelerations. The proposed signal-processing framework is verified against a practical railway case study using an open-access reference dataset [10].

The remainder of this paper is organized as follows. Section 2 details the signal-processing methodology; Section 3 introduces the experimental dataset and reports the corresponding results; and Section 4 synthesizes the main findings and delineates potential avenues for future research.

2 Methodology

The proposed methodology establishes a deterministic link between the discrete spatial coordinates provided by the GNSS and the high-frequency dynamic responses captured by the IMU. The workflow resolves the inherent discrepancies in sampling rates and reference frames through a sequence of kinematic derivations, decimation filtering, and linear transformations. The methodology partitions the processing architecture into ten primary stages, summarized in Table 1.

Step	Description
1. GNSS data pre-processing	Load GNSS data (latitude, longitude, altitude, time); interpolate to uniform temporal sampling;
2. Data purging	Identify and remove zero-velocity and duplicated GNSS samples.
3. Coordinate conversion	Convert geodetic WGS84 coordinates to local Cartesian frame.
4. Uniform spatial resampling	Define uniform distance vector; interpolate positions, velocities, and times as a function of distance.
5. GNSS position filtering	Apply low-pass filter to smooth trajectory.
6. GNSS lateral acceleration estimation	Derive velocity via central differences; decompose acceleration into tangential and normal (lateral) components.
7. IMU data pre-processing	Load triaxial accelerometer and gyroscope data; align IMU time to match GNSS duration; resample to uniform step.
8. Decimation filtering	Apply a low-pass filter followed by downsampling to reduce IMU rate to GNSS rate.
9. Accelerometer frame alignment	Estimate transformation matrix that aligns IMU and GNSS estimated data.
10. Lateral accelaration estimation from gyroscope	Compute lateral acceleration from IMU yaw-rate channel.

Table 1: Data processing workflow for lateral acceleration comparison.

2.1 GNSS data management and processing

The GNSS receiver outputs geodetic quantities referenced to the World Geodetic System 1984 (WGS84) reference ellipsoid [11]. The unprocessed measurements are arranged into a geodetic matrix $\mathbf{G}$, containing latitude, longitude, and ellipsoidal height, and an associated time-stamp vector $\boldsymbol{t}_g$, as shown in Equation 1.

$$\mathbf{G} = \begin{bmatrix} \mathrm{lat}_0 & \mathrm{lon}_0 & \mathrm{elev}_0 \\ \mathrm{lat}_1 & \mathrm{lon}_1 & \mathrm{elev}_1 \\ \vdots & \vdots & \vdots \\ \mathrm{lat}_{N_g} & \mathrm{lon}_{N_g} & \mathrm{elev}_{N_g} \end{bmatrix}, \qquad \boldsymbol{t}_g = \begin{bmatrix} t_{g_0} \\ t_{g_1} \\ \vdots \\ t_{g_{N_g}} \end{bmatrix}. \tag{1}$$

where $(N_g + 1)$ is the total number of GNSS samples.

The geodetic coordinates contained in $\mathbf{G}$ are mapped onto a local cartesian reference frame to enable subsequent kinematic analysis. The resulting spatial coordinates are assembled in the matrix $\mathbf{X}$, while the associated uniformly sampled time instants are stored in the vector $\mathbf{t}$, as reported in Equation 2.

$$\mathbf{X} = \begin{bmatrix} x_0 & y_0 & z_0 \\ x_1 & y_1 & z_1 \\ \vdots & \vdots & \vdots \\ x_{N_c} & y_{N_c} & z_{N_c} \end{bmatrix}, \qquad \boldsymbol{t} = \begin{bmatrix} t_0 \\ t_1 \\ \vdots \\ t_{N_c} \end{bmatrix}, \tag{2}$$

where $(N_c + 1)$ is the total number of cartesian interpolated samples.

2.2 Kinematic information and lateral acceleration from GNSS

A central-difference numerical scheme is applied to discrete position samples in $\mathbf{X}$ to compute velocities and accelerations. The resulting signals are then passed through a low-pass filter to reduce high-frequency noise caused by numerical differentiation, consistent with the relatively low sampling rate of the GNSS receiver. Equation 3 gives the velocity estimates and Equation 4 the accelerations, both in time t_k.

$$\boldsymbol{v}_k = \frac{\mathbf{x}_{k+1} - \mathbf{x}_{k-1}}{t_{k+1} - t_{k-1}}, \quad k \geq 1, \tag{3}$$

where $\boldsymbol{x}_k = \begin{bmatrix} x_k & y_k & z_k \end{bmatrix}^\intercal$ and t_k are the Cartesian position vector and the time sample, respectively.

$$\boldsymbol{a}_k = \frac{2}{t_{k+1} - t_{k-1}} \left(\frac{\mathbf{x}_{k+1} - \mathbf{x}_k}{t_{k+1} - t_k} - \frac{\mathbf{x}_k - \mathbf{x}_{k-1}}{t_k - t_{k-1}} \right), \quad k \geq 1. \tag{4}$$

The method decomposes the total acceleration $\boldsymbol{a}_k$ into tangential ($\boldsymbol{a}_t$) and normal ($\boldsymbol{a}_n$) components shown in Equation 5. These signals follow the dynamic frame of the railway (longitudinal forward x, lateral left y, vertical up z) according to the SAE J670e [12] and ISO 8855 [13] standards.

$$\begin{cases} \boldsymbol{a}_{t_k} = \boldsymbol{a}_k \, \hat{\boldsymbol{v}}_k^\intercal \hat{\boldsymbol{v}}_k \\ \boldsymbol{a}_{n_k} = \boldsymbol{a}_k - \boldsymbol{a}_{t_k} \end{cases} \Rightarrow \begin{cases} a_{g_{x_k}} = \|\boldsymbol{a}_{t_k}\| - g\sin(\phi_k) \\ a_{g_{y_k}} = \|\boldsymbol{a}_{n_k}\| \,\mathrm{sgn}\big(\begin{bmatrix} 0 & 0 & 1 \end{bmatrix} (\boldsymbol{v}_k \times \boldsymbol{a}_{n_k})\big), \\ a_{g_{z_k}} = -g\cos(\phi_k) \end{cases} \tag{5}$$

where $g = 9.81\ \mathrm{m/s^2}$ is the gravitational acceleration constant, $\hat{\boldsymbol{v}}_k$ the unitary velocity vector and ϕ_k is the instantaneous track gradient, shown in Equation 6.

$$\phi_k = \arctan\left(\frac{z_{k+1} - z_{k-1}}{\sqrt{(x_{k+1} - x_{k-1})^2 + (y_{k+1} - y_{k-1})^2}}\right). \tag{6}$$

The GNSS-based estimate of lateral acceleration corresponds to the component a_{kg_y} in Equation 5, which expresses the lateral acceleration in the dynamic reference frame of the vehicle. Equation 7 defines the GNSS acceleration matrix $\mathbf{A}_{\mathrm{GNSS}}$.

$$\mathbf{A}_{\mathrm{GNSS}} = \begin{bmatrix} \mathbf{a}^{\mathsf{T}}_{\mathrm{GNSS}_0} \\ \mathbf{a}^{\mathsf{T}}_{\mathrm{GNSS}_1} \\ \vdots \\ \mathbf{a}^{\mathsf{T}}_{\mathrm{GNSS}_{N_c}} \end{bmatrix}, \tag{7}$$

where $\boldsymbol{a}^{\mathsf{T}}_{\mathrm{GNSS}_k} = \begin{bmatrix} a_{g_{x_k}} & a_{g_{y_k}} & a_{g_{z_k}} \end{bmatrix}$ is the acceleration vector at sample time t_k.

2.3 IMU data management

The IMU dataset consists of triaxial accelerometer and gyroscopic measurements. The accelerometer signals are collected in the matrix $\mathbf{A}_{\mathrm{IMU}}$, while the gyroscope angular rate measurements about the z-axis are stored in the vector $\boldsymbol{z}_{\mathrm{rate}}$. The corresponding sampling instants are represented by the time vector $\boldsymbol{t}_i$. These quantities are summarized in Equation 8.

$$\mathbf{A}_{\mathrm{IMU}} = \begin{bmatrix} \boldsymbol{a}^{\mathsf{T}}_{\mathrm{IMU}_0} \\ \boldsymbol{a}^{\mathsf{T}}_{\mathrm{IMU}_1} \\ \vdots \\ \boldsymbol{a}^{\mathsf{T}}_{\mathrm{IMU}_{N_i}} \end{bmatrix}, \qquad \boldsymbol{z}_{\mathrm{rate}} = \begin{bmatrix} z_{\mathrm{rate}_0} \\ z_{\mathrm{rate}_1} \\ \vdots \\ z_{\mathrm{rate}_{N_i}} \end{bmatrix}, \qquad \boldsymbol{t}_i = \begin{bmatrix} t_{i_0} \\ t_{i_1} \\ \vdots \\ t_{i_{N_i}} \end{bmatrix}, \tag{8}$$

where $\mathbf{a}^{\mathsf{T}}_{\mathrm{IMU}_k} = \begin{bmatrix} a_{i_{x_k}} & a_{i_{y_k}} & a_{i_{z_k}} \end{bmatrix}$ is the IMU acceleration vector at sample time t_k and $(N_i + 1)$ is the total number of IMU samples.

2.4 Decimation filtering for IMU-GNSS time synchronization

A central challenge in multi-sensor railway monitoring arises from the pronounced discrepancy between the sampling frequencies of the GNSS and IMU subsystems. In the reference data set under consideration, the acquisition rates are $f_{\mathrm{GNSS}} = 1$ Hz and $f_{\mathrm{IMU}} = 500$ Hz, corresponding to a sampling-rate ratio of 500:1. Any direct comparison of these two data streams without prior temporal alignment or resampling would lead to significant aliasing effects and, consequently, would invalidate the physical interpretability of any derived cross-sensor correlations.

The synchronization procedure follows the classical decimation paradigm, which consists of two sequential operations. The first operation is anti-aliasing low-pass filtering. Before any downsampling, a finite-impulse-response (FIR) low-pass filter processes the high-rate IMU signal and sets the cut-off frequency f_c below the Nyquist frequency of the target GNSS rate, as given by Equation 9:

$$f_c \leq \frac{f_{\text{GNSS}}}{2}. \tag{9}$$

This step is critical: omitting the anti-aliasing filter would fold high-frequency IMU content (rail corrugation, wheel-flat impacts, etc.) into the low-frequency band, corrupting the lateral acceleration signal.

The second operation is integer-factor downsampling. The method downsamples the filtered signal by retaining every d-th sample, where Equation 10 defines the decimation factor d.

$$d = \frac{f_{\text{IMU}}}{f_{\text{GNSS}}}. \tag{10}$$

For the present dataset, $d = 500$. This procedure produces the decimated IMU acceleration matrix $\mathbf{A}_{D_{\text{IMU}}}$, whose length matches the GNSS data vector. After decimation, the method computes a uniform trajectory-length stamp to establish the spatial alignment between the IMU and GNSS accelerations. Figure 1 illustrates the y-axis IMU signal before and after the decimation process.

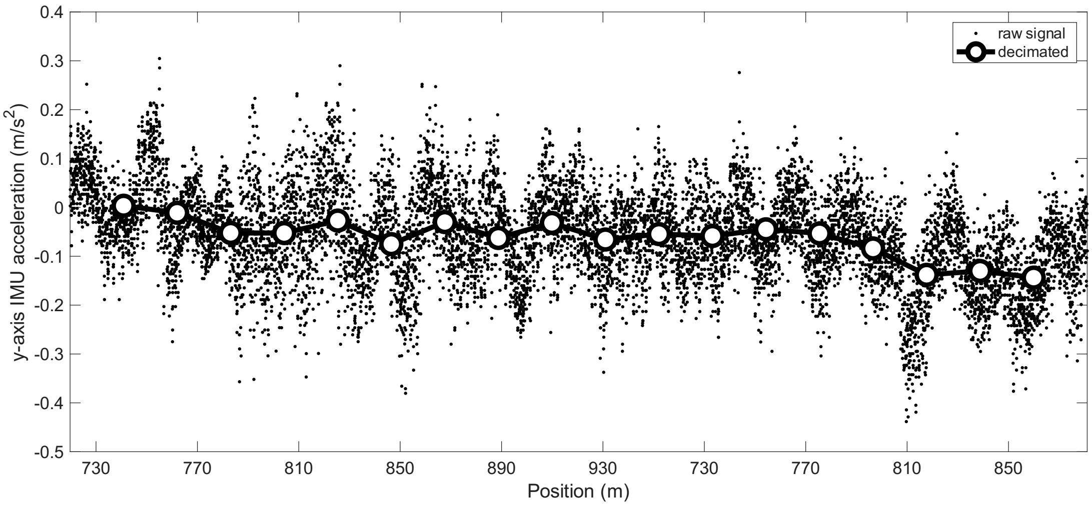

Figure 1: Decimation filtering result for y-axis IMU acceleration: raw 500 Hz signal overlaid on data downsampled to 1 Hz.

2.5 Lateral acceleration from IMU gyroscope z-axis angular rate

The IMU gyroscope kinematic signature provides an alternative and independent estimate of the lateral acceleration. Equation 11 describes how a vehicle accelerates laterally while it travels at longitudinal speed v_x along a curved path with z-axis angular rate $\dot{\psi}$.

$$a_{\psi_y} = v_x \dot{\psi}. \tag{11}$$

where ψ is the Yaw or z-axis angle

2.6 Coordinate-frame alignment and conditioning

A further linear transformation is applied to the decimated IMU matrix $\mathbf{A}_{D_{\mathrm{IMU}}}$ in order to align it to the GNSS dynamic frame. This operation is achieved through the transformation matrix $\mathbf{M}$, which embeds rotation, translation, and scale-factor corrections, via least squares as given by Equation 12:

$$\mathbf{M} = \hat{\mathbf{A}}_{\mathrm{GNSS}}^{\mathsf{T}} \left(\hat{\mathbf{A}}_{D_{\mathrm{IMU}}}^{\mathsf{T}} \right)^{+}, \tag{12}$$

where $\hat{\mathbf{A}}_{\mathrm{GNSS}}^{\mathsf{T}}$ is the transposed homogenized GNSS acceleration matrix and $\left(\hat{\mathbf{A}}_{D_{\mathrm{IMU}}}^{\mathsf{T}} \right)^{+}$ is the Moore-Penrose pseudoinverse of the transposed homogenized decimated IMU matrix. The homogenized matrices are built from the original acceleration matrices, adding an extra column of 'ones' after the last column of each matrix.

Equation 13 then defines the conditioned acceleration matrix:

$$\mathbf{A}_{\mathrm{IMU_{cond}}} = \hat{\mathbf{A}}_{D_{\mathrm{IMU}}} \mathbf{M}^{\mathsf{T}} \begin{bmatrix} 1 & 0 & 0 \\ 0 & 1 & 0 \\ 0 & 0 & 1 \\ 0 & 0 & 0 \end{bmatrix}. \tag{13}$$

This process ensures that all three lateral accelerations a_{i_y} (IMU acceleration), a_{g_y} (GNSS estimated), and a_{ψ_y} (gyroscope IMU) are expressed in the same coordinate frame and at the same sampling rate, allowing for a physically meaningful comparison.

3 Results

The validation employs the open-access railway dataset [10], which provides a standardized baseline to assess the performance and reliability of the GNSS-IMU processing algorithms. The instrumentation suite reflects standard industry specifications. The GNSS receiver logs the geodetic coordinates at $f_{\mathrm{GNSS}} = 1$ Hz. The IMU accelerometers and gyroscopes operate at $f_{\mathrm{IMU}} = 500$ Hz, giving a decimation factor $d = 500$. The data acquisition system (DAQ) uses a synchronized logging architecture with GNSS time-stamping to minimize inter-sensor latency. The railway track in the dataset spans a 10 km path as shown in Figure 2.

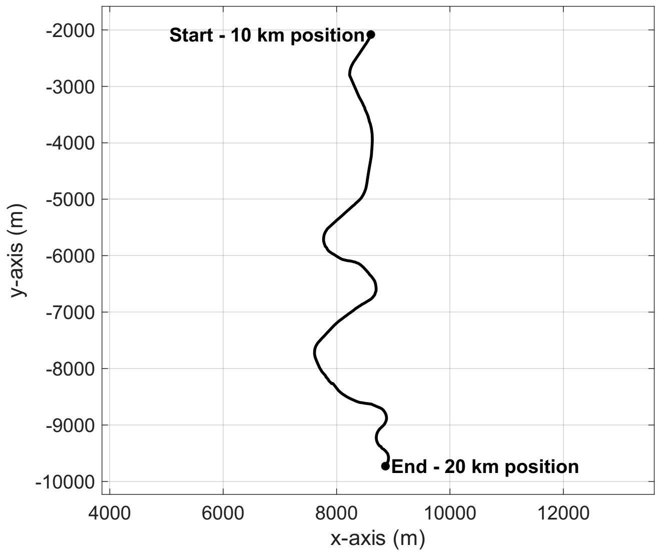

Figure 2: Railway cartesian path.

Figure 3 presents a comparison of the three estimates of lateral acceleration along the 10 km test segment.

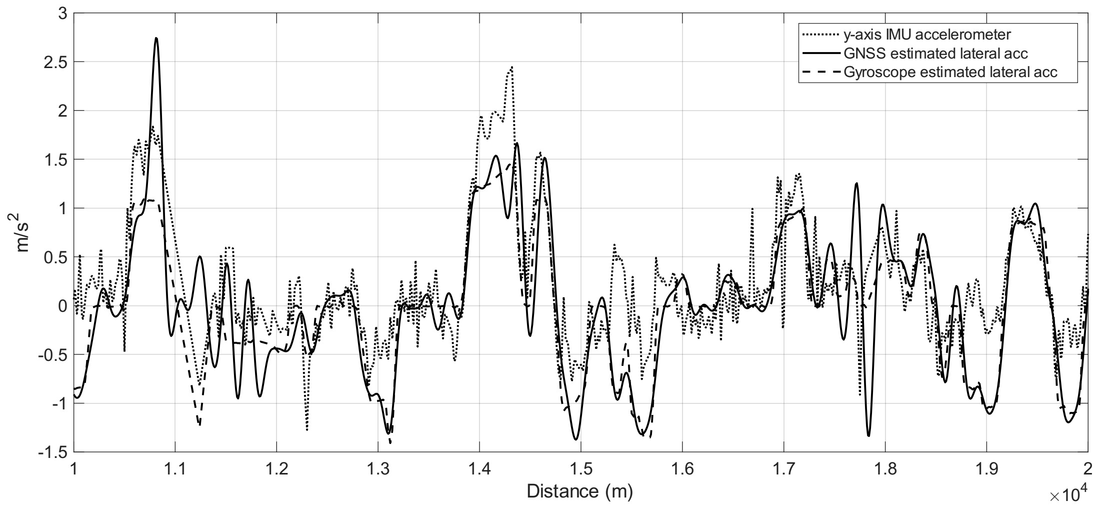

Figure 3: Comparison of lateral accelerations from three sources.

3.1 Comments of Results

The distance aligned lateral acceleration profiles presented in Figure 3 exhibit the same general expected behavior. However, it is evident that the GNSS estimates show better consistency with the gyroscope derived measurements. In contrast, the accelerometer lateral accelerations frequently display discrepancies in both magnitude and, in some instances, sign relative to the other two estimates. This behavior clearly indicates the influence of local track characteristics, such as superelevation, rail misalignment, or other features of interest that may arise under normal or degraded operating conditions.

4 Conclusions

This study has presented a deterministic signal-processing framework for the comparative analysis of lateral acceleration in railway environments using three independent estimation methods: direct IMU accelerometer measurement, GNSS kinematic derivation, and gyroscope readings. The methodology addresses the fundamental challenge of multi-rate sensor fusion through a decimation filtering procedure.

The proposed methodology enabled a comparative evaluation of acceleration estimates along the alignment of a railway segment. The three independent acceleration sources can be exploited to perform detailed analyses of both track and vehicle conditions under realistic operational circumstances.

Future research will focus on developing robust statistical metrics for quantifying the agreement between the three estimation paths, extending the framework to multi-sensor fusion architectures, and constructing high-reliability lateral acceleration databases for advanced railway diagnostic analysis.

Acknowledgements

The authors thank the School of Mechanical Engineering (FEM) of the University of Campinas (UNICAMP) and the Federal Institute of São Paulo (IFSP) for institutional support and grant funding for doctoral studies.

References

[1] Z. Orbán and S. Váradi, "Study on the dynamics of a freight train and its interaction with the track," *Technologies*, vol. 12, no. 1, p. 14, 2024. DOI: 10.3390/technologies12010014.

[2] A. Yaliniz and A. Erden, "Evaluation of rail surface defects with accelerometers," in *2020 Innovations in Intelligent Systems and Applications Conference (ASYU)*, 2020, pp. 1–5. DOI: 10.1109/ASYU50717.2020.9259880.

[3] S. Jłudek, K. Karwowski, and A. Wilk, "Preparatory research on determining the vertical profile of railway tracks using inertial sensors," *Sensors*, vol. 22, no. 11, p. 4096, 2022. DOI: 10.3390/s22114096.

[4] S. Chen, Y. Wu, and Y. Song, "Railway track irregularity estimation using car-body vibration based on Kalman filter," *South African Journal of Industrial Engineering*, vol. 36, no. 3, pp. 187–198, 2018. DOI: 10.1080/10233393.2018.1506541.

[5] J. González-Carbajal and J. L. Escalona, "Estimation of rail track geometry using inertial sensors on in-service trains," in *14th International Conference on Education and New Learning Technologies*, 2022. DOI: 10.21125/edulearn.2022.0645.

[6] Y. Zhou and X. Zhang, "Prediction of railway track irregularities based on long short-term memory networks," *Journal of Rail and Rapid Transit*, 2025.

[7] M. Espindola and A. A. Santos, "Analysis of dynamic interaction between railway vehicles and track using machine learning," *Railway Engineering Science*, 2026.

[8] H. Hadj-Mabrouk, "Contributions of artificial intelligence to railway safety," *Safety Science*, 2026.

[9] A. Pires, G. F. M. dos Santos, and A. A. dos Santos Junior, "Identificação de irregularidades de via permanente através de acelerômetros embarcados," in *Anais do XI Congresso Nacional de Engenharia Mecânica*, São Paulo, 2022.

[10] R. Winter *et al.*, "Rail surface defect detection through vibration analysis," *Applied Sciences*, vol. 10, 2020.

[11] S. Kumar, "World survey of wheel/rail forces," *Vehicle System Dynamics*, vol. 21, pp. 144–183, 1988.

[12] SAE International, *Vehicle Dynamics Terminology*, SAE J670, Standard, 2022.

[13] International Organization for Standardization, *ISO 2631-1:1997/Amd 1:2010*, Standard, 2011.